Research on Flow Characteristics of Electronically Controlled Injection Device Developed for High-Power Natural Gas Engines

Binbin Sun, Wenqing Ge, Yongjun Wang, Cao Tan & Bo Li*

School of Transportation and Vehicle Engineering, Shandong University of Technology, 255049, Zibo, Shandong, China
*E-mail: sdutlibo@126.com

Abstract. Accurate fuel supply is a key factor that influences the performance of high-power natural gas engines. The premixed and single-point natural gas supply system is the most commonly used method to ensure a large fuel supply but one of its shortcomings is the inaccuracy of the fuel supply. A new type of natural gas injection device with fungiform configuration and electronically controlled actuator was developed to achieve high efficiency and stable operation in high-power natural gas engines. Firstly, a computational fluid dynamics (CFD) model of the injection device was created. Based on this model, the key structure parameters that have a significant influence on the outlet flow were confirmed. A particle swarm optimization (PSO) model was developed to identify the optimal outflow structure. Then, a flow function for precise flow supply control was constructed based on a response surface model, according to the flow rates of the device under different control parameters. Finally, a flow-characteristic test bench and a high-power engine prototype were developed to verify the simulation and optimization results. The results indicate that the optimized outflow structure shows low pressure loss and a large flow rate, improving injection efficiency by 10.37% and mass flow by 11.78% under 0.4 Mpa pressure difference. More importantly, the cycle fuel supply could be controlled accurately for each cylinder owing to the developed flow function. Consequently, compared with the original engine using a single-point natural gas supply system, the cylinder performance imbalance was improved by 37.47%.

Keywords: *electronic control natural gas injection device; flow function; high-power natural gas engine; optimization of outlet structure.*

1 Introduction

Confronted with the increasingly serious petroleum energy crisis and environmental pollution, development of energy-saving and emission-reducing technology has become a trend in the engine industry [1]. Compared with fuel-oil engines, natural gas engines have the specific advantages of higher efficiency and lower emissions, especially greenhouse gas emission [2,3].

Received December 12th, 2018, Revised February 25th, 2019, Accepted for publication July 8th, 2019.
 ISSN: 2337-5779, DOI: 10.5614/j.eng.technol.sci.2019.51.4.1

Natural gas is one of the most widely used clean burning fuels in large bore engines [4,5]. Owing to the research on efficiency improvement and emission reduction in natural gas engines, innovative concepts, such as high-energy ignition, exhaust gas recirculation, multi-point and intermittent fuel injection, etc., have been developed [6-8]. While each concept has its advantages and limitations, multi-point and intermittent fuel injection has proved to be a very effective tool to improve engine performance [9].

In comparison with the premixed and single-point natural gas supply system [10], an electronically controlled multi-point fuel supply system can provide accurate and real-time controllable natural gas supply required by each cylinder, which improves engine performance significantly [11]. Currently, multi-point fuel supply systems are widely used in vehicle natural gas engines to meet the requirements of increasingly stringent regulations. Many studies have been conducted on the system's development and optimization [12].

However, for large bore natural gas engines used in specific places, such as coal mines, oil fields, large ships, etc., the premixed and single-point natural gas supply system is still commonly used to meet the requirement of large fuel supply. This fuel supply method inevitably leads to poor stability, low efficiency and high emissions [13]. Consequently, electronically controlled injection devices with fungiform configuration to achieve large fuel outflow have been developed for the multi-point fuel supply system [14-16]. Magnetic field design, controller development and motion performance optimization have been conducted for a new type of natural gas injection device, achieving excellent performance. Nevertheless, the details of the outlet flow characteristics, which influence the cycle fuel supply optimization and precise control, are still unknown.

In this study, the outlet flow characteristics of a new type of natural gas injection device with fungiform configuration were investigated. Firstly, the characteristics of four outflow structures were analyzed based on the CFD method. Then, the outflow structure of the injection device was optimized based on a CFD model and the PSO algorithm. Moreover, a flow function for injection control was constructed based on an analysis of the flow rates under different control parameters. Finally, a test bench for outlet flow characteristics and a high-power natural gas engine prototype were developed to verify the theoretical models.

2 Flow Characteristics of the Fungiform Configuration

This section presents an analysis of the design of a gaseous injection device, aimed at low pressure loss and high flow rate, with four outlet structures. A

complex optimization platform consisting of a genetic algorithm and CFD was developed to confirm the optimal outlet structure. Finally, the optimized scheme was analyzed.

2.1 Influence of Outlet Structure on Flow Characteristics

2.1.1 Design of Four Outlet Structures

According to the principle of the injector with the characteristic of critical velocity [17], as shown in Figure 1, four outlet structures were designed to investigate the influence of the structure parameters on the flow characteristics, especially gular diameter and diffusion tube length. As shown in Figure 1, structures a and c are designed with the same gular diameter and inlet angle (θ_1), but with different diffusion tube length and outlet angle (θ_2). There is no diffusion tube or outlet angle in structure c.

The structural characteristics of structures b and d are similar to those of structures a and c. The difference between structures a and b is the gular diameter, which is also applicable to structures c and d. Based on the above design, the influence of the diffusion tube length on the flow characteristics can be confirmed by the comparison of structures a and c with structures b and d. Furthermore, based on the analysis of structures a and b, the influence of gular diameter on flow characteristics could be obtained.

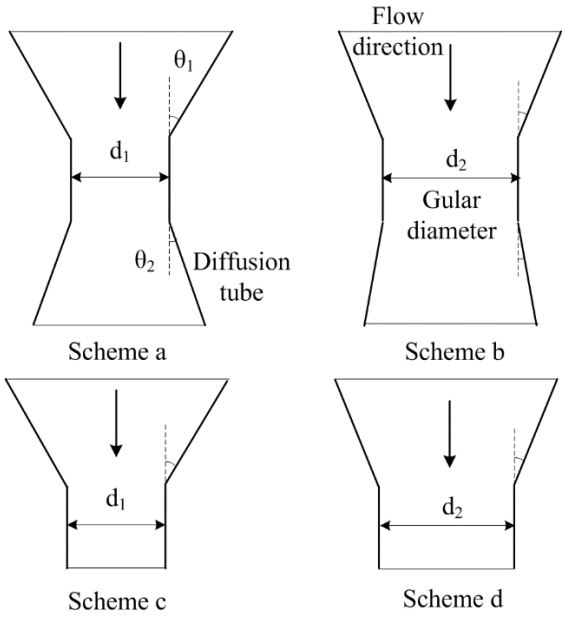

Figure 1 Scheme of the four outlet structures.

2.1.2 Design of CFD Model

To analyze the influence of the outlet structure parameters on the flow characteristics, the software applications Catia, Gambit and Fluent were used.

First of all, using the Catia software, the three-dimensional structure of the injection device was designed as shown in Figure 2(a). Then, as shown in Figure 2(b), the computational domain for the CFD model was created according to the structure model. A pressure stabilizing cavity was designed for investigation of the characteristics of the outlet flow field.

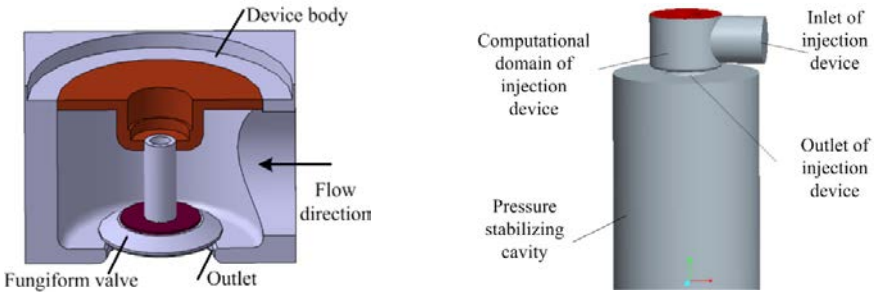

(a) Three-dimensional structure

(b) Computational domain

Figure 2 Three-dimensional model and computational domain of the injection device.

Furthermore, the Gambit software application was used to generate the grid of the computational domain. To simulate steady state condition for example, given the valve lift at different pressure differences, the static structured mesh and the unstructured mesh were gridded according to a regular structure and an irregular structure, as shown in Figure 3(a). Moreover, as shown in Figure 3(b), to simulate the opening and closing of the valve, a structured mesh was designed for grid updating.

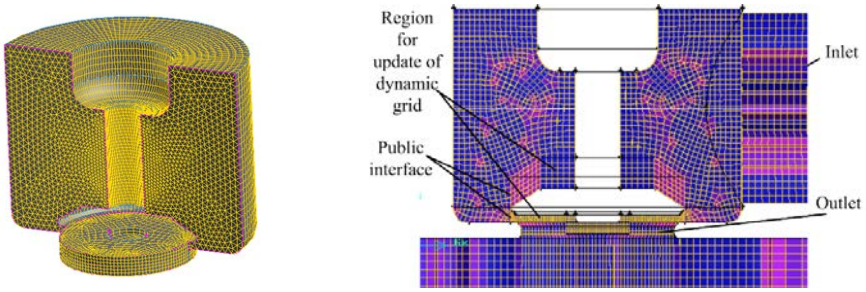

(a) Static mesh of flow region

(b) Dynamic mesh of flow region

Figure 3 Static mesh and dynamic mesh for CFD calculation.

The slippage grid method was used to disconnect the public interface between the static mesh and the dynamic mesh. This method was used to transfer data and at the same time avoid negative mesh. Dynamic layering was used to update the mesh in the dynamic region. Finally, the Fluent software application was used for calculating the flow characteristics in the computational domain based on the following equations.

Specifically, the mass conservation equation in Eq. (1) was used.

$$\frac{\partial \rho}{\partial t}+\frac{\partial(\rho u)}{\partial x}+\frac{\partial(\rho v)}{\partial y}+\frac{\partial(\rho w)}{\partial z}=0 \tag{1}$$

where ρ is the density of the flow, t is time, u, v and w mean the velocity components on the x, y and z axes, respectively.

The momentum conservation equation in Eq. (2) was used.

$$\begin{cases} \rho\dfrac{\mathrm{d}u}{dt}=\rho F_{bx}+\dfrac{\partial p_{xx}}{\partial x}+\dfrac{\partial p_{yx}}{\partial y} \\ \rho\dfrac{\mathrm{d}v}{dt}=\rho F_{by}+\dfrac{\partial p_{xy}}{\partial x}+\dfrac{\partial p_{yy}}{\partial y}+\dfrac{\partial p_{zy}}{\partial z} \\ \rho\dfrac{\mathrm{d}w}{dt}=\rho F_{bz}+\dfrac{\partial p_{xz}}{\partial x}+\dfrac{\partial p_{yz}}{\partial y}+\dfrac{\partial p_{zz}}{\partial z} \end{cases} \tag{2}$$

where F_{bx}, F_{by} and F_{bz} are the force components on the x, y and z axes, respectively, p is the stress tensor and the subscript indicates the component of the stress tensor.

The energy conservation equation in Eq. (3) was used.

$$\frac{\partial(\rho T)}{\partial t}+div(\rho u T)=div\left(\frac{k}{c_p}grad(T)\right)+S_T \tag{3}$$

where T is the temperature of the fluid, k is the thermal conductivity, c_p is the specific heat capacity, S_T is the viscous dissipation.

Moreover, the standard k-ε model was used to calculate the turbulence characteristics of natural gas.

$$\begin{cases} \rho\dfrac{dk}{dt}=[(\mu+\dfrac{\mu_t}{\sigma_k})\dfrac{\partial k}{\partial x_i}]+G_k+G_b-\rho\varepsilon-Y_M \\ \rho\dfrac{d\varepsilon}{dt}=[(\mu+\dfrac{\mu_t}{\sigma_\varepsilon})\dfrac{\partial \varepsilon}{\partial x_i}]+C_{1\varepsilon}\dfrac{\varepsilon}{k}(G_k+C_{3\varepsilon}G_b)-C_{2\varepsilon}\rho\dfrac{\varepsilon^2}{k} \end{cases} \tag{4}$$

where G_k and G_b mean the turbulent kinetic energy caused by average velocity gradient and buoyancy, respectively, Y_m characterizes the influence of compressible turbulent on dissipation rate, u_t is the turbulence viscosity coefficient, and $C_{1\varepsilon}$, $C_{2\varepsilon}$, σ_k and σ_ε are the constant coefficients.

The inlet and outlet boundary conditions of the CFD model were set as pressure inlet and pressure outlet boundary conditions. The outlet pressure was confirmed based on the pressure in the intake manifold. Consequently, the inlet pressure was set according to the pressure difference. The temperature boundary condition was 298 K. The wall boundary condition was adiabatic.

2.1.3 Influence of Structure Parameters on Flow Characteristics

The simulation result is shown in Figure 4. The difference in flow rate between structures a and c is very small, which also applies to structures b and d. The calculation result indicates that the influence of the diffusion tube on the flow rate is insignificant. Moreover, based on the comparison between structure a and b it is obvious that the gular diameter has a significant influence on the flow rate.

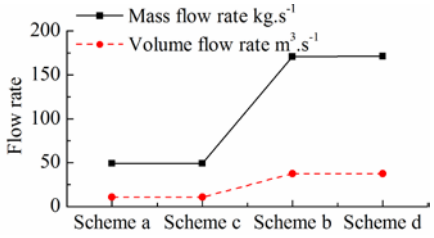

Figure 4 Flow rates of the four outlet structures.

To investigate the influence of the outlet structure on the pressure loss and the natural gas velocity, the former affects the injection efficiency and the latter affects the fuel movement intensity. The pressure and movement characteristics of structures b and d were calculated as shown in Figure 5. It can be concluded that the outlet structure without diffusion tube (structure d) reduces pressure loss, which improves injection efficiency. Furthermore, the gas velocity at the outlet port of structure d is higher than that of structure b, which means greater gas movement intensity is achieved without diffusion tube.

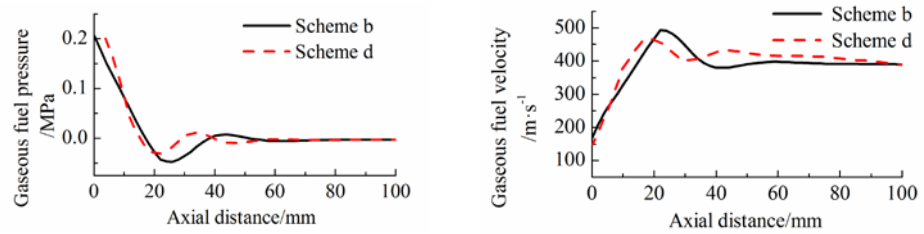

(a) Change of natural gas pressure (b) Change of natural gas velocity

Figure 5 Influence of diffusion tube on natural gas pressure and velocity.

2.2 Optimization of the Outlet Structure

Based on the discussion of the influence of the structure parameters on the flow characteristics, the structure parameters of the injection device shown in Figure 6 were optimized. In order to reduce the cost of optimization, as shown in Figure 7, an off-line optimization program based on the PSO algorithm and a CFD model were designed to optimize the outlet.

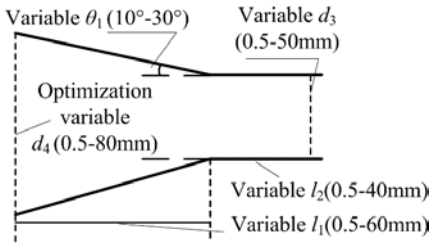

Figure 6 Optimization variables of the injection device.

The details of the optimization are as follows. First of all, according to the flying range of the particles (the optimization variables), a random particle swarm is formatted. The flight ranges of the designed particles are related to their effective values. According to the optimization parameters designed above, the flying range of particles was designed in Eq. (5).

$$\begin{cases} 10^\circ \le \theta_1 \le 30^\circ \\ 0.5\text{mm} \le d_3 \le 50\text{mm} \\ 0.5\text{mm} \le d_4 \le 80\text{mm} \\ 0.5\text{mm} \le l_1 \le 60\text{mm} \\ 0.5\text{mm} \le l_2 \le 40\text{mm} \end{cases} \tag{5}$$

In order to convert the optimization variables to PSO particles, the variables are deduced as shown in Eq. (6).

$$\begin{cases} \begin{bmatrix} \left(x_{1\_\theta_1}, x_{1\_d_3}, x_{1\_d_4}, x_{1\_l_1}, x_{1\_l_2}\right) \\ \cdots \\ \left(x_{n\_\theta_1}, x_{n\_d_3}, x_{n\_d_4}, x_{n\_l_1}, x_{n\_l_2}\right) \end{bmatrix} \\ \begin{bmatrix} \left(v_{1\_\theta_1}, v_{1\_d_3}, v_{1\_d_4}, v_{1\_l_1}, v_{1\_l_2}\right) \\ \cdots \\ \left(v_{n\_\theta_1}, v_{n\_d_3}, v_{n\_d_4}, v_{n\_l_1}, v_{n\_l_2}\right) \end{bmatrix} \end{cases} \tag{6}$$

where v represents the particle velocity, x means the particle position, n is the population size.

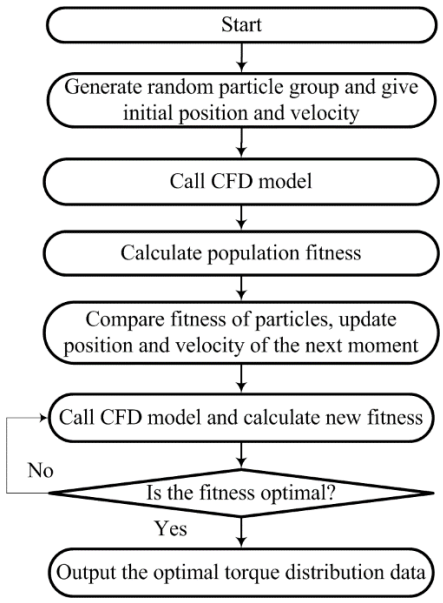

Figure 7 Off-line optimization for outlet structure based on PSO.

Secondly, in each iteration step, the PSO particles are imported into the CFD model to calculate the actual pressure in the injection device. Based on the kinematic equation of one-dimensional isentropic non-steady air [18], the relationship between actual pressure and stagnation pressure is calculated as shown in Eq. (7).

$$\frac{p}{p_0} = (1 + \frac{k-1}{2} M_a^{\ 2})^{\frac{k}{k-1}} \tag{7}$$

where p_0 is the stagnation pressure, p is the actual pressure of an arbitrary cross section, M_a is the Mach number, k is the isentropic index; the isentropic indexes of air and methane are 1.4 and 1.3 respectively.

To quantify the influence of pressure loss, the injection efficiency based on the injection pressure was designed as shown in Eq. (8).

$$e_p = \frac{p_{o,eff}}{p_{o,nom}} \tag{8}$$

where e_p is injection efficiency, $p_{o,eff}$ is effective stagnation pressure, and $p_{o,nom}$ is the stagnation pressure of the injection device at the inlet port.

Based on the injection efficiency function, the fitness value of any particle (θ_{1_i}, d_{3_i}, d_{4_i}, l_{1_i}, l_{2_i}) is confirmed at any given moment.

$$f_{it\_i}(t) = e_{p\_i} = \frac{p_{o,eff\_i}}{p_{o,nom\_i}} \tag{9}$$

Then, the fitness value of any particle is compared with two factors, i.e. the optimum value that the particle has experienced and the optimum value experienced by the particle group. According to the comparison results, the speed and direction of any particle are updated.

$$\begin{cases} v_i(t+1) = kv_i(t) + k\varphi_1 p_{se1}(t)\left[f_{it\_in}(t) - x_i(t) \right] \\ \qquad\qquad + k\varphi_2 p_{se2}(t)\left[f_{it\_to}(t) - x_i(t) \right] \\ x_i(t+1) = x_i(t) + v_i(t+1) \end{cases} \tag{10}$$

where $v(t)$ represents the particle velocity at moment t, $x(t)$ means the particle position at moment t, φ_1 and φ_2 are learning factors used to adjust the particle to the best position, p_{se1} and p_{se2} represent independent pseudorandom numbers that ensure the randomness of particle search; k is the convergence factor, $f_{it\_in}(t)$ and $f_{it\_to}(t)$ are the optimal fitness values of the particle and the population at moment t, respectively.

Finally, by repeating the iteration step discussed above, the optimal particle positions are obtained, i.e. θ_1 is 18.2°, d_3 is 16.4 mm, d_4 is 41.8mm, l_1 is 5.7 mm and l_2 is 5.3 mm.

2.3 Analysis of the Optimized Scheme

Based on the pressure and velocity distributions presented in Figures 8 and 9 it could be confirmed that the outlet structure has a significant influence on the

flow characteristics. Specifically, with the original scheme there is a relatively large pressure loss caused by the diffusion cube, which leads to negative pressure in the intake manifold of the engine.

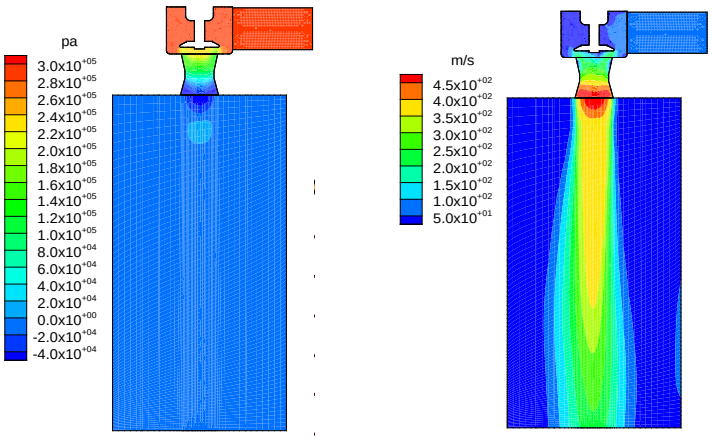

(a) Pressure nephogram (b) Velocity nephogram

Figure 8 Pressure and velocity of the original outlet structure.

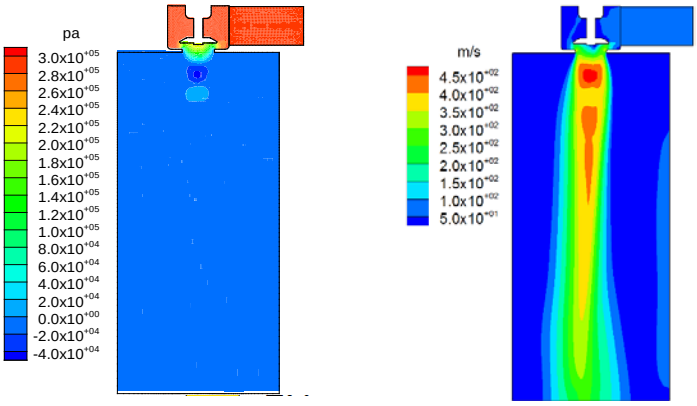

(a) Pressure nephogram (b) Velocity nephogram

Figure 9 Pressure and velocity of the optimized outlet structure.

As shown in Figure 10, axial distance means a straight length from the outlet port in the axis interface. In the original scheme, the outlet-port pressure is negative, while in the optimized scheme the pressure is still positive, which helps to improve the injection efficiency and avoid inverse flow. The main reason for the improvement of the outlet-port pressure is optimization of the outlet structure. In comparison with the original scheme, the increase of the outflow angle reduces the local windage loss, while the supersonic flow causes no negative pressure.

Furthermore, compared with the original outlet structure, the new scheme improves the natural gas velocity. As shown in Figure 10, owing to the larger outflow angle and shorter expansion length, both the local loss and the route loss are reduced. Consequently, there is still natural gas with high velocity at some distance from the outlet port, which is useful for improving the mixture of air and fuel.

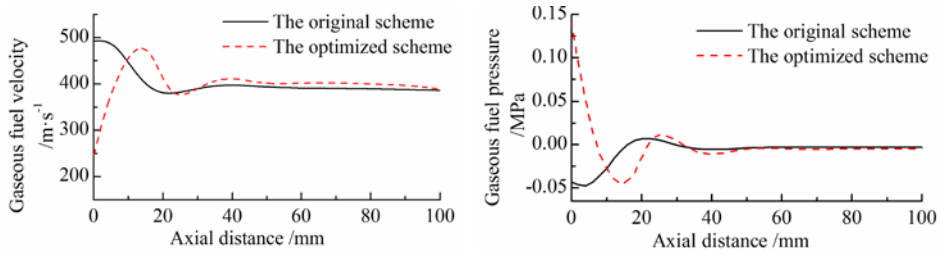

(a) Natural gas velocity (b) Natural gas pressure

Figure 10 Change of natural gas velocity and pressure.

From the mass flow rate shown in Figure 11(a) it is obvious that the optimized outlet structure of the injection device is conducive to improving the mass flow rate. Under the simulation condition where the pressure difference between the inlet and outlet is 0.4 Mpa, the mass flow rate of the new structure is increased by 11.78% in comparison with the original one. According to the kinematic equation of one-dimensional isentropic non-steady air, the injection efficiency of the new-type outlet structure is 64.2%, i.e. an increase by 10.37% in comparison with the original scheme. The main reason is that the Maher number per mass of the optimized scheme is greater because of the optimized hollow throat. Furthermore, based on the law of energy conservation, in the optimized scheme, higher injection efficiency means less local loss and route loss. Consequently, the smaller pressure loss leads to a higher pressure distribution of the injection chamber and an increase of the mass flow rate.

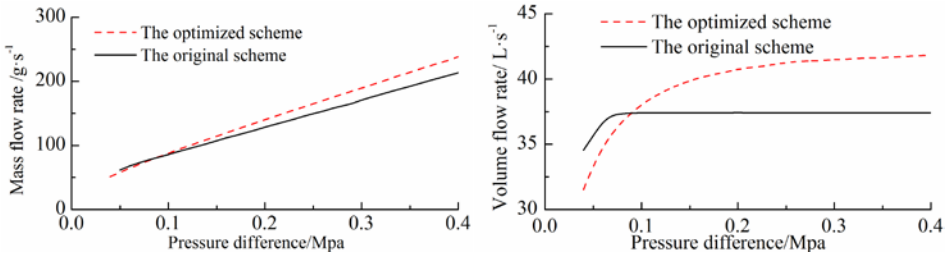

(a) Mass flow rate of different schemes (b) Volume flow rate of different schemes

Figure 11 Flow characteristics of the original and the optimized scheme.

Furthermore, the optimized structure also has a positive effect on the volume flow rate, as shown Figure 11(b). However, different from the mass flow rate, which changes linearly with the pressure difference, the relationship between the volume flow rate and the pressure difference is nonlinear after about 0.1 Mpa. Consequently, in this study, a mass flow cure was used to control the natural gas injection to achieve accurate mass flow.

3 Flow Function of the Injection Device

For the mass flow rate under single cycle shown in Figure 12, greater volatility of mass flow occurs during the valve open period and stable mass flow can be achieved when the valve stays open. The simulation result shows that the mass flow rate is 85.6 $g.s^{-1}$ when the pressure difference between inlet and outlet is 0.1 Mpa and the maximum valve lift is 4 mm.

The pressure difference and the valve lift are the key factors that affect the mass flow rate. To quantify the influence of pressure difference and valve lift on mass flow rate, the orthogonal test method was adopted. The pressure difference was designed within 0.04 Mpa and 0.14 Mpa to match the air pressure in the intake manifold of the high-power engine; the pressure difference interval from 0.04 Mpa to 0.14 Mpa was 0.01 Mpa; the maximum valve lift interval from 1 mm to 4 mm was 1 mm. The mass flow rate of the injection device was calculated under each operation. Figure 13 presents the simulated mass flows of the operation designed above. It is obvious that the mass flow rate is directly proportional to the pressure difference and the valve lift.

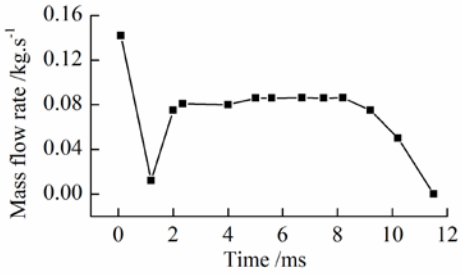

Figure 12 Flow rate curve of the pressure inlet of the injection device.

Based on the response surface method [19], the mass flow rate as a function of pressure difference and valve lift was developed to control the cycle natural gas mass for each cylinder of the high-power engine. Furthermore, the R^2 and RMSE of the mass flow rate model were confirmed as 0.9996 and 0.5462, respectively, which means the modeling accuracy is high enough for engineering application.

$$q_m = -0.27h^3 + 0.16h^2 - 18.87h^2\Delta p + 255.6h\Delta p + 11.02h - 30.39\Delta p + 1.03 \quad (11)$$

where h is the valve lift of the injection device, $\triangle p$ is the pressure difference between the inlet and outlet of the injection device, q_m is the mass flow rate.

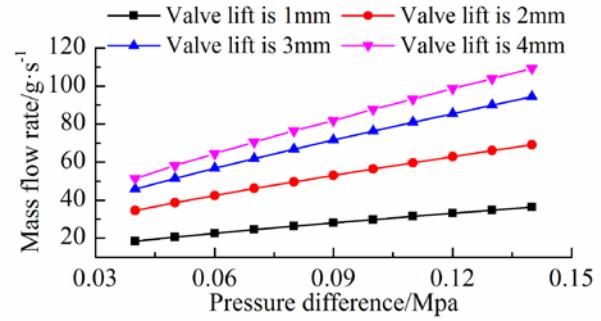

Figure 13 Variation of mass flow rate and volume flow.

4 Verification

To verify the CFD simulation result and the mass flow function for injection control, a flow characteristic test bench for the injection device was developed, as shown in Figure 14.

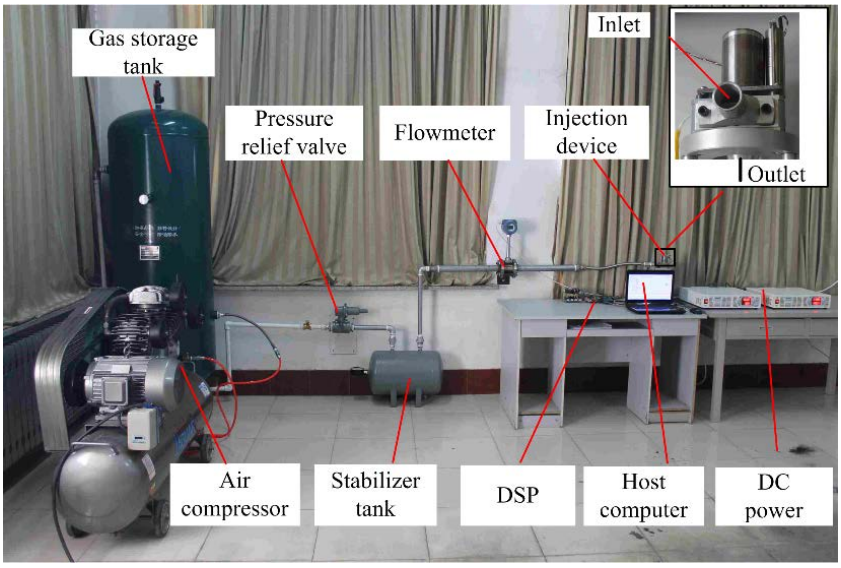

Figure 14 Flow characteristic test bench of the injection device.

The air compressor was designed for achieving a high pressure difference. To provide a continuous and stable gas supply, a gas storage tank and a stabilizer tank were used. A pressure relief valve was adopted to control the pressure difference between the inlet and outlet. A flow meter was used to test the dynamic airflow. The injection device system consisted of DSP, injection device, host computer and DC power. The DSP was used to collect the signals and control the valve motion. Control command and the test result were achieved by the host computer. DC power was designed for the power supply of the DSP and the sensor in the injection device.

To ensure data reliability for any operation designed by orthogonal method, the actual mass flow rate was tested ten times and the average value was adopted. The various pressure differences were achieved by regulating the pressure relief valve. As the verification result in Figure 15 shows, the errors between the calculated mass flow rate and the actual results were all within 4%, which means that the CFD model and the mass flow rate function have high accuracy and can be used for cycle mass injection control.

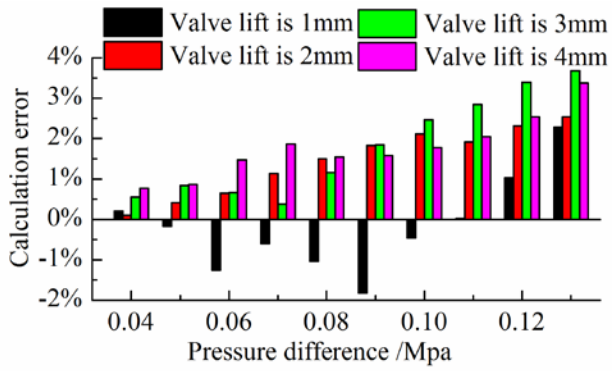

Figure 15 Calculation error of the developed function calculating mass flow rate.

Moreover, to verify the influence of cycle mass injection controlled by the mass flow rate function on the engine's performance, a high-power engine test platform was developed, as shown in Figure 16. The details of the engine parameters are presented in Tables 1 and 2. An electric generator was driven by the natural gas engine to generate electricity for a coal mine. Monitoring equipment was used for the acquisition of the engine signals. To test cylinder performance imbalance, twelve WRNK-291 thermocouples and twelve Kistler 2516 in-cylinder pressure sensors were used. Their details are presented in Table 2. The multi-point injection system, consisting of twelve injection

devices, a DSP system, DC power and a host computer, was developed for the control of natural gas supply.

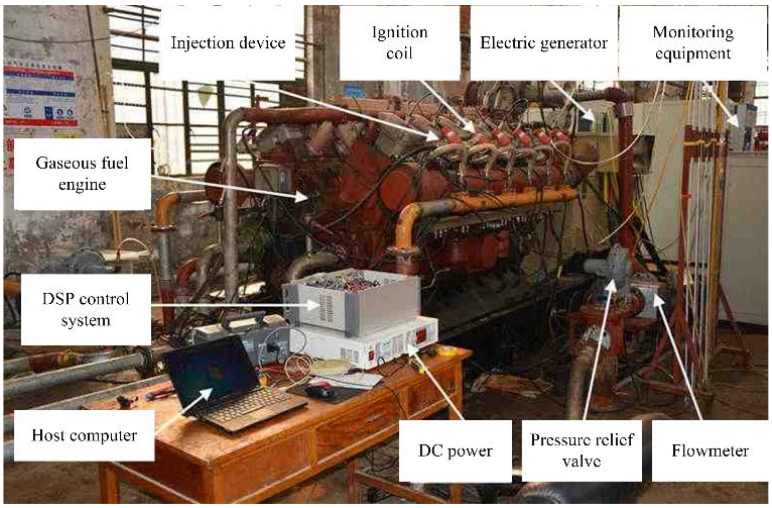

Figure 16 Engine prototype with multi-point fuel supply system.

Table 1 Parameters of the high-power engine.

Items	Parameters or type
Engine type	V type
Stroke	Four strokes
Intake mode of air	Supercharge
Cylinder number	12
Cylinder diameter × stroke /mm	190×210
Compression ratio	11:1
Intake timing parameter /°CA	324~596
Exhaust timing parameter /°CA	127~399
Rated power /kW	680
Rated power /r·min^{-1}	1000

Table 2 Parameters of pressure sensor and thermocouple.

Kistler 2516 in-cylinder pressure sensor		WRNK-291 thermocouple	
Items	**Values**	**Items**	**Values**
Measuring range / MPa	0~25	Measuring range / ℃	0-1000
Input voltage /V	1~15	Input voltage /V	5~15
Sensitivity /(V/MPa)	0.07~0.4	Accuracy /℃	±2.5
Accuracy /MPa	0.01	Thermal response time/s	3~5
Operating temperature of charge amplifier /℃	0~50	Insulation resistance in room temperature/MΩ	≥500

In high-power natural gas engines, cylinder performance imbalance will lead to unstable operation with bad economy, emission and dynamic performances. The original natural gas supply system used the premixed and single-point supply technology. The uncontrollable fuel mass of each cylinder has an adverse influence on the cylinder performance balance. In the test prototype, the natural gas was supplied by an electrically controlled multi-point injection system. The maximum valve lift of the injection device was 4 mm. The pressure relief valve was designed to control the pressure of the natural gas. The injection time changed with cylinder operation and the cycle mass of natural gas for each cylinder was controlled by the mass flow rate function.

The exhaust temperature is a key factor for indicating cylinder performance imbalance. More importantly, the exhaust temperature of each cylinder can be measured easily with the use of a temperature sensor. Consequently, in this study, the exhaust temperatures of the twelve cylinders were tested to analyze the influence of the fuel supply system on engine performance.

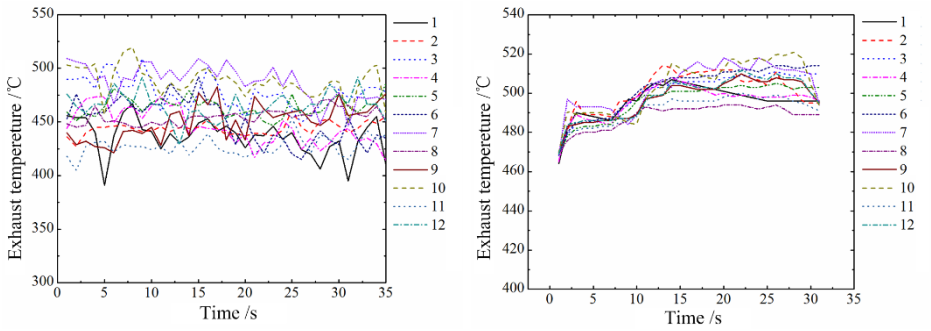

(a) The original scheme (b) The optimized scheme

Figure 17 Characteristics of exhaust temperature in each cylinder.

As shown in Figure 17, under the operation that the engine speed was at 700 r.min^{-1} and the throttle was fully open, the exhaust temperatures of the twelve cylinders were measured. It is obvious that, in comparison with the original natural gas supply system, the proposed injection system with fungiform valve and high-performance outlet structure could better meet the cycle fuel mass requirement of the high-power engine. More importantly, based on the mass flow rate function developed above, the high-power engine improved the cylinder performance balance owing to accurate cycle fuel mass control. However, influenced by the natural gas with time-variant proportion of methane, the cylinder performance balance of the newly developed engine still needs to be improved. More specifically, future research work will focus on the development of correction control of the time-variant natural gas.

To quantitatively analyze the influence of the developed natural gas injection system on cylinder performance balance, a function indicating the exhaust temperature volatility of each cylinder was developed as follows:

$$C_0V(T) = \sigma(T) / \overline{T} \times 100\% \tag{12}$$

$$\sigma(T) = \sqrt{\frac{1}{i-1}\sum_{j=1}^{i}(Ti - \overline{T})^2} \tag{13}$$

$$\overline{T} = \frac{1}{i}\sum_{j=1}^{i} T_i \tag{14}$$

where i means the number of cylinders, $\sigma(T)$ is the standard deviation of exhaust temperatures, $\overline{T}$ is the average exhaust temperature of the twelve cylinders.

Under the operation that the engine speed was at 700 r.min^{-1} and the throttle was fully open, the exhaust temperature volatility of the original engine was 4.27%, which is higher than that of the newly developed engine (2.67%). The cylinder performance imbalance was improved by 37.47% owing to the multi-point fuel injection system with the optimized outlet structure.

5 Conclusions

In this study, a new type of natural gas injection device with fungiform configuration was designed for large-bore engines. Based on PSO and CFD, the influence of the outlet structure on the flow characteristics was analyzed and optimized. Bench tests were conducted on the injection device. According to the simulation and test results, the following conclusions can be drawn.

1. The electronically controlled multi-point fuel supply system was able to improve engine performance. The single-point fuel supply system, which is still commonly used in large-bore engines, is limited by the low flow rate of the conventional injection device with needle valve or ball valve, which has a negative effect on engine performance. The injection device with fungiform outlet structure proposed in this paper showed perfect performance in flow characteristics. The large flow rate of the injection device can meet the cycle-fuel requirement of large-bore engines. Consequently, in comparison with a single-point fuel supply stem, the cylinder performance imbalance was improved by 37.47% owing to accurate fuel control of the multi-point fuel supply system.
2. The outlet structure has a significant influence on the flow characteristics of the injection device. Based on the CFD method and the PSO algorithm, the

key structure parameters of the device were optimized and perfect performance was achieved. Owing to the optimized structure, under a pressure difference between the inlet and outlet of 0.4 Mpa, the injection efficiency and the mass flow rate were improved by 10.37% and 11.78% respectively.

3. Compared with the mass flow rate, which changes linearly with the pressure difference, the relationship between volume flow rate and pressure difference shows nonlinearity, which actually increases complexity for cycle-fuel injection control. Consequently, based on the response surface method, the mass flow rate was designed as a function of pressure difference and valve lift. The R^2 and RMSE of the function were 0.9996 and 0.5462 respectively, which means that the accuracy of the function is high enough for engineering application.

Acknowledgements

This work was supported by the National Natural Science Foundation Project of China (51875326, 51805301), the Natural Science Foundation Project of Shandong (ZR2019BEE043), the Zibo City-Shandong University of Technology Cooperative Projects, China (2017ZBXC165), the Zhangdian-Shandong University of Technology Cooperative Projects, China.

References

[1] Energy Strategy Research Group of Chinese Academy of Sciences field, *Roadmap of Chinese Energy Technology Development for 2050*, 1st ed., Social Sciences Academic Press, pp 1-10, 2015.

[2] Pasymi, Y.W.B. & Yazid B., *Axial Inlet Geometry Effects on the Flow Structures in a Cyclone Burner Related to the Combustion Performance of Biomass Particles*, Journal of Engineering and Technological Sciences, **50**(5), pp. 684-697, 2018.

[3] Ou, X. & Zhang, X., *Life-Cycle Analyses of Energy Consumption and GHG Emissions of Natural Gas-Based Alternative Vehicle Fuels in China*, Journal of Energy, **2013**, pp. 1-9, 2013.

[4] Tsujimura T. & Suzuki Y., *Development of a Large-Sized Direct Injection Hydrogen Engine for a Stationary Power Generator*, International Journal of Hydrogen Energy, **44**(22), pp. 11355-11369, 2018.

[5] Sidarto K.A., Kania A. & Mucharam L., *Determination of Gas Pressure Distribution in A Pipeline Network Using the Broyden Method*, Journal of Engineering and Technological Sciences, **49**(6), pp. 750-769, 2017.

[6] Li, H., Haugen, G. & Ditaranto, M., *Impacts of Exhaust Gas Recirculation (EGR) on the Natural Gas Combined Cycle Integrated with Chemical Absorption CO_2 Capture Technology*, Energy Procedia, **4**, pp. 1411-1418, 2011.

[7] Pundle, A., *Modeling and Analysis of the Formation of Oxides of Nitrogen and Formaldehyde in Large-Bore, Lean-Burn, Natural Gas Engines*, Master's Dissertation, Mechanical Engineering, University of Washington, Washington, United States, 2013.

[8] Hekkert, M.P., Hendriks, F.H.J.F. & Faaij, A.P.C., *Natural Gas as an Alternative to Crude Oil in Automotive Fuel Chains Well-to-Wheel Analysis and Transition Strategy Development*, Energy Policy, **33**, pp. 579-594, 2005.

[9] Hyunjun, P., Sanghuk, L., Jinyeong, J. & Chang, D., *Design of the Compressor-assisted LNG Fuel Gas Supply System*, Energy, **158**, pp. 1017-1027, 2018.

[10] Boretti, A., Lappas, P. & Zhang, B., *CNG Fueling Strategies for Commercial Vehicles Engines - A Literature Review*, in SAE 2013 World Congress, SAE Technical Paper 2013-01-2812, 2013. DOI: 10.4271/2013-01-2812.

[11] Zhao, Q., Ni, C. & Zhang, Y., *Experiment Study of The Single Point and Multi-Point Natural Gas Electronic Injection System*, Applied Mechanics and Materials, **313-314**, pp. 479-483, 2013. DOI: 10.4028/www.scientific.net/AMM.313-314.479.

[12] Adolf, M., Bargende, M. & Becker, M., *Vehicle Development for Natural Gas and Renewable Methane*, Springer International Publishing, 2nd ed., pp. 229-458, 2016.

[13] Ruter, M.D., Olsen, D.B., Scotto, M.V. & Perna, M.A., *Performance of a Large Bore Natural Gas Engine with Reformed Natural Gas Prechamber Fueling*, in Proceedings of the ASME 2010 Internal Combustion Engine Division Fall Technical Conference, pp. 83-91, 2010. DOI: 10.1115/ICEF2010-35162.

[14] Ge, W., Liu, L. & Chang, S., *Design of an Electronically Controlled Injection Device for Heavy-Duty Gas Engine*, China Mechanical Engineering, **22**, pp. 2768-2771, 2012.

[15] Ge, W., Zhao, Y. & Li, B., *Numerical Simulation of Electric Controlled Injection Device Equipped on Gas Fuel Engine*, Journal of Networks, **9**(7), pp. 1948-1954, 2014. DOI: 10.4304/jnw.9.7.1948-1954.

[16] Chang, S. & Ge, W., *An Electronically Controlled Injection Device for Gas Fuel*, Patent for Invention of China, 2011.

[17] Chang, F., *Uncertainty Analysis of Gas Flow Standard Device with Critical Flow Venturi Nozzle Method*, China Petroleum and Chemical Standard and Quality, 2011.

[18] Wang, T., Liu, L. & Chang, S., *Steady-flow Characteristic of Gas Fuel Injection Device*, China Mechanical Engineering, **26**(15), pp. 2041-2046, 2015.
[19] Sun, B., Li, B., Wang, Y. Ge, W. & Gao, S., *Development of Drive Control Strategy for Front-and-Rear-Motor-Drive Electric Vehicle (FRMDEV)*, Journal of Engineering and Technological Sciences, **50**(5), pp. 720-736, 2018.